UC Irvine
UC Irvine Previously Published Works

Title

A Novel In Vivo Approach to Assess Radial and Axial Distensibility of Large and Intermediate Pulmonary Artery Branches

Permalink

https://escholarship.org/uc/item/8jp9c3xd

Journal

Journal of Biomechanical Engineering, 137(4)

ISSN

0148-0731

Authors

Bellofiore, A
Henningsen, J
Lepak, CG
et al.

Publication Date

2015-04-01

DOI

10.1115/1.4029578

Peer reviewed

A Novel In Vivo Approach to Assess Radial and Axial Distensibility of Large and Intermediate Pulmonary Artery Branches

A. Bellofiore
Department of Biomedical Engineering,
University of Wisconsin-Madison,
Madison, WI 53706-1609;
Department of Chemical,
Biomedical and Materials Engineering,
San José State University,
San José, CA 95192-0082

J. Henningsen
Department of Biomedical Engineering,
University of Wisconsin-Madison,
Madison, WI 53706-1609

C. G. Lepak
Department of Biomedical Engineering,
University of Wisconsin-Madison,
Madison, WI 53706-1609

L. Tian
Department of Biomedical Engineering,
University of Wisconsin-Madison,
Madison, WI 53706-1609

A. Roldan-Alzate
Department of Radiology,
University of Wisconsin-Madison,
Madison, WI 53792-3252

H. B. Kellihan
Department of Veterinary Medicine,
University of Wisconsin-Madison,
Madison, WI 53706-1102

D. W. Consigny
Department of Radiology,
University of Wisconsin-Madison,
Madison, WI 53792-3252

C. J. Francois
Department of Radiology,
University of Wisconsin-Madison,
Madison, WI 53792-3252

N. C. Chesler[1]
Department of Biomedical Engineering,
University of Wisconsin-Madison,
2146 ECB, 1550 Engineering Drive,
Madison, WI 53706-1609
e-mail: chesler@engr.wisc.edu

Pulmonary arteries (PAs) distend to accommodate increases in cardiac output. PA distensibility protects the right ventricle (RV) from excessive increases in pressure. Loss of PA distensibility plays a critical role in the fatal progression of pulmonary arterial hypertension (PAH) toward RV failure. However, it is unclear how PA distensibility is distributed across the generations of PA branches, mainly because of the lack of appropriate in vivo methods to measure distensibility of vessels other than the large, conduit PAs. In this study, we propose a novel approach to assess the distensibility of individual PA branches. The metric of PA distensibility we used is the slope of the stretch ratio–pressure relationship. To measure distensibility, we combined invasive measurements of mean PA pressure with angiographic imaging of the PA network of six healthy female dogs. Stacks of 2D images of the PAs, obtained from either contrast enhanced magnetic resonance angiography (CE-MRA) or computed tomography digital subtraction angiography (CT-DSA), were used to reconstruct 3D surface models of the PA network, from the first bifurcation down to the sixth generation of branches. For each branch of the PA, we calculated radial and longitudinal stretch between baseline and a pressurized state obtained via acute embolization of the pulmonary vasculature. Our results indicated that large and intermediate PA branches have a radial distensibility consistently close to 2%/mmHg. Our axial distensibility data, albeit affected by larger variability, suggested that the PAs distal to the first generation may not significantly elongate in vivo, presumably due to spatial constraints. Results from both angiographic techniques were comparable to data from established phase-contrast (PC) magnetic resonance imaging (MRI) and ex vivo mechanical tests, which can only be used in the first branch generation. Our novel method can be used to characterize PA distensibility in PAH patients undergoing clinical right heart catheterization (RHC) in combination with MRI. [DOI: 10.1115/1.4029578]

Keywords: pulmonary artery stiffness, pulmonary arterial hypertension, vascular biomechanics, magnetic resonance angiography, digital subtraction angiography

Introduction

PAH is an incurable disease of the distal pulmonary vasculature. Progressive narrowing and obliteration of the small PAs is responsible for increased resistance to blood flow and subsequent elevation in PA pressure. A hallmark of PAH is the progressive loss of compliance of the proximal PAs [1–3], which along with the increased resistance contributes to aggravate right ventricular (RV) afterload [2,4–7], eventually leading to RV failure.

Loss of compliance of the PAs has been assessed via either total PA compliance [2] or area strain of the main PA [4,8]. These metrics of PA stiffness have strong prognostic value in patients with PAH [4,8], suggesting PA stiffness is an important contributor to the pulsatile component of RV workload [9,10]. However, with the exception of the first generation of PA branches (left and right extralobar PAs), which only contribute to 20% of total PA compliance [11], distensibility of individual branches of the PAs cannot currently be assessed in vivo. Differences in PA distensibility among generations of PA branches may have clinical relevance and be important to mechanisms of PAH progression.

A common metric of local distensibility is the slope α of the stretch ratio–pressure relationship for a given PA. If PA distensibility is assumed to be constant throughout the PAs [12], a single value of α for the entire PA network can be obtained based on interpolation of multipoint pressure-flow data [13–16]. This global α is about 2%/mmHg in healthy subjects independent of age [16,17]. In patients with PAH, a decrease in global PA distensibility was negatively correlated with PA pulse pressure [13], which in turn is responsible for endothelial cell dysfunction and further arterial stiffening [7,18]. Global PA distensibility α was significantly decreased in healthy carriers of the BMPR-2 mutation, a precursor of PAH [19], thus suggesting a sensitivity of α to early
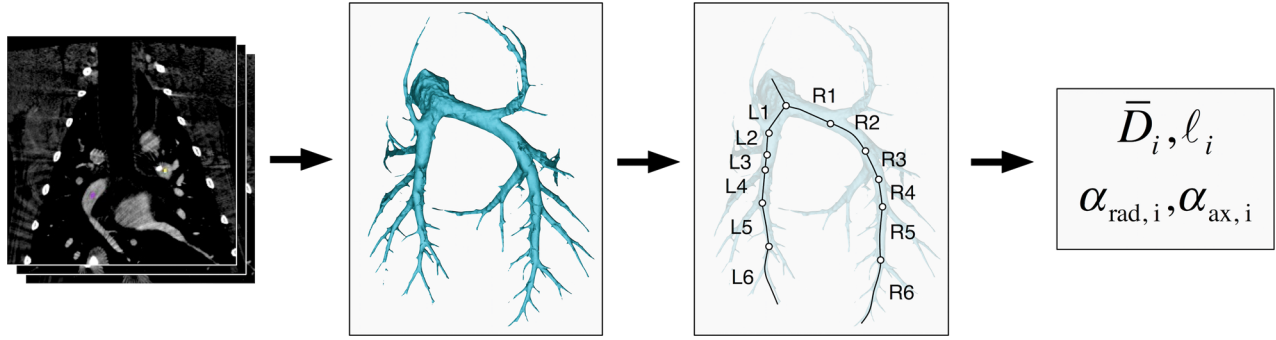
Fig. 1 Flow chart of the process used to assess radial and axial distensibility from angiographic images. Stacks of 2D images, obtained with either CT-DSA or CE-MRA, were segmented to reconstruct 3D surface models of the PA network. Radial and axial distensibility were calculated for the first six branch generations. Note that in the text the branches R1 and L1 indicate the extralobar RPA and LPA, respectively.

pathological changes in PAH [20,21]. Whether differences in local α exist within the pulmonary network in healthy or diseased states remains unknown, largely because techniques to measure PA branch α in vivo do not exist.

In this study, we propose a novel method to evaluate the distensibility of individual PA branches in vivo. Under the assumption that the stretch ratio–pressure relationship is approximately linear in the physiological range of PA pressures, the slope α can be estimated for each branch of the PA if strain and pressure are known at two different stretch levels. Our method combines measurements of PA pressure from RHC and geometry of individual PA branches from either computed tomography angiography or magnetic resonance angiography. In six healthy female dogs, we performed these measurements at baseline and after acute embolization of the PA to calculate radial and axial distensibility of the PAs. We compared our in vivo radial distensibility data with ex vivo measurements from mechanical tests.

Methods

RHC. In vivo and ex vivo data were collected from six female beagles. The animals were approximately 1 year of age and their body weight was 8.3 ± 2.4 (mean $\pm$ standard deviation). Under general anesthesia and 100% oxygen ventilation, the animals underwent MRI, computed tomography angiography, and RHC twice, first to obtain PA hemodynamic and morphometric data at baseline (PRE) and second to measure the same parameters after acute elevation of PA pressure via embolization (POST). Surgical procedures are described in more detail elsewhere [22]. Briefly, the external jugular vein was catheterized to place a fluid-filled pressure catheter for measuring PA pressure and cardiac output via thermodilution. The same access was used to repeatedly inject polyvinyl alcohol microbeads (Contour SE Microspheres, Boston Scientific, Natick, MA) into the right atrium. PA pressure was measured intermittently and bead injection was continued until mean PA pressure was greater than 30 mmHg. Dogs were euthanized after the POST tests. All the procedures were approved by the Institutional Animal Care and Use Committee (IACUC) of the University of Wisconsin-Madison. After euthanasia, extralobar PAs were harvested for mechanical testing.

CT-DSA. Flat-detector computed tomography angiography [23,24] was performed on a C-arm flat-panel detector scanner (Artis Zeego, Siemens, Germany). The acquisition included a mask run (no contrast) and a fill run (contrast-enhanced). The contrast agent (60 ml of Imeron 400) was injected into the right atrium at 5 ml/s, followed by 60 ml of saline flush. Acquisition parameters were: acquisition time 20 s/run, 70 kV, 512×512 matrix, projection on 30×40 cm flat panel size, 200 deg total angle, 0.4 deg/frame, 496 frames total, dose 1.2 μGy/frame. The fill run acquisition was triggered to the detection of the arrival of the

contrast bolus. A dedicated program (DynaCT, Siemens, Germany) was used to acquire and postprocess the angiographic data. Postprocessing included reconstruction of both mask run and fill run. Digital subtraction was performed to obtain CT-like projections (8-mm thickness, 1-mm spacing) to visualize the pulmonary vasculature. Ventilation was suspended during the scan (breath hold) to prevent respiration-induced motion artifacts.

CE-MRA. CE-MRA was performed on a clinical 3.0 T scanner (MR750, GE Healthcare, Waukesha, WI) with gradients operating in Zoom mode (40 mT/m gradient strength, 150-mT/m/ms slew rate). Intravenous contrast (0.10 mmol/kg of gadobenate dimeglumine) was administered at 2 ml/s, followed by 25 ml of saline flush. Acquisition was performed during the steady state after the administration of contrast. Parameters were adjusted to optimize spatial resolution, acquisition duration and vascular contrast-to-noise-ratio. CE-MRA parameters were: $34 \times 30 \times 27.2$ cm field of view, $256 \times 200 \times 180$ matrix, ± 83.3 kHz bandwidth, TR/TE $= 3.4/1.1$ ms (fractional echo), and flip angle of 25 deg, for a true spatial resolution of $1.3 \times 1.5 \times 1.5$ mm. Autocalibrating reconstruction for Cartesian acquisition with an acceleration factor of 3.75 was used to reduce the acquisition time. CE-MRA was performed during end expiration.

Radial and Axial Distensibility. Stacks of 2D images of the pulmonary vasculature (from CT-DSA or CE-MRA) were analyzed using Mimics 15 (Materialise, Leuven, Belgium) to reconstruct 3D surface models of the PA network. The image analysis is summarized in Fig. 1. Image thresholding was performed to segment the PA network. Segmentation threshold was selected manually for each dataset to include as many PA branches as possible while still allowing the PAs to be isolated from veins. The 3D model was further refined to isolate the PAs using standard editing tools. The principal left and right arterial pathways were identified and centerlines were calculated by using an algorithm available in the MedCAD Mimics module. Major branching points were chosen to divide each pathway into arterial segments. Starting the bifurcation distal to the main PA, segments were selected down to the sixth generation for each pathway. For each generation, branch length and average best-fit diameters were calculated for the PRE and POST data. Radial distensibility α_{rad} was calculated dividing the radial strain by the increase in mean PA pressure as follows:

$$\alpha_{rad} = \frac{D_{POST} - D_{PRE}}{D_{PRE}(\bar{P}_{POST} - \bar{P}_{PRE})} \qquad (1)$$

where D_{PRE} and D_{POST} are the average best-fit diameter of the PA branch at baseline and after embolization, respectively, and $\bar{P}_{PRE}$

and $\bar{P}_{POST}$ are the corresponding values of mean PA pressure. Similarly, the axial distensibility α_{ax} was calculated as

$$\alpha_{ax} = \frac{\ell_{POST} - \ell_{PRE}}{\ell_{PRE}(\bar{P}_{POST} - \bar{P}_{PRE})} \qquad (2)$$

where ℓ_{PRE} and ℓ_{POST} are the length of the PA branch at baseline and after embolization, respectively.

PC MRI. MRI studies were performed on a clinical 3 T scanner (MR750, GE Healthcare, Waukesha, WI) using an eight-channel cardiac coil and vector electrocardiographic (ECG) gating. 2D PC images were acquired in double oblique planes through the left PA (LPA) and right PA (RPA). Image parameters for 2D PC imaging were: 35×26 cm field of view, 256×160 matrix, 7 mm slice, ± 62.5 kHz bandwidth, 150 cm/s velocity encode ("venc"), TR/TE = 5.5/2.6 ms (full echo), and segmentation factor of 8, for a true temporal resolution of 44 ms. Twenty interpolated time frames were reconstructed. One slice was acquired while suspending ventilation for approximately 15–17 s.

In order to measure cross-sectional area of the LPA and RPA, the 2D PC images were analyzed using the CV Flow analysis tool (Medis, Leiden, The Netherlands). The LPA and RPA contours were segmented manually on the magnitude images over the entire cardiac cycle to evaluate the cross-sectional area A. For each phase of the cardiac cycle, the branch diameter was calculated as $D = \sqrt{4A/\pi}$. The cycle-average diameters $\bar{D}_{PRE}$ and $\bar{D}_{POST}$ were used to calculate α_{rad} with Eq. (1).

Mechanical Tests. After euthanasia, the intact large proximal PAs were harvested and any connective tissue was removed before a photograph was taken of the intact PAs to measure PA length ex vivo. Next, a short ring from each PA (LPA and RPA) was cut and opened, and its cross section was photographed for measuring the geometry of the artery at its stress-free state. The cut-open ring was taken as the circumferentially oriented specimen for uniaxial testing. The specimen was clamped by self-aligning grips on each end in an Instron 5548 MicroTester tensile testing system (Instron, Norwood, MA), equipped with a 10 N load cell. The tissue specimen was immersed in phosphate-buffered saline (PBS) at 37 °C in an environmental chamber throughout the test.

For each specimen, the stress–stretch curve was used to evaluate an equivalent ex vivo radial distensibility α to be compared with the in vivo data (α_{rad}). The in vivo circumferential stress σ corresponding to the mean PA pressure ($\bar{P}$) measured in vivo was calculated using the law of Laplace, as follows:

$$\sigma = \frac{\bar{P} \times D}{2h} \qquad (3)$$

where D and h are, respectively, the inner diameter and thickness of the PA branch at pressure $\bar{P}$. While the inner diameter (D) was obtained from in vivo CT-DSA measurements, the wall thickness (h) was calculated with the incompressibility condition using the PA geometry at the stress-free state, the in vivo inner diameter, and the in vivo axial stretch. The in vivo axial stretch of each PA (LPA and RPA) at baseline or after embolization was calculated as the ratio of the in vivo PA length measured from CT-DSA at baseline or after embolization to the reference PA length measured from ex vivo photograph. With the in vivo circumferential stress calculated by Eq. (3), the corresponding circumferential stretch was found from the stress–stretch curve obtained from mechanical testing. The radial distensibility from ex vivo mechanical data was calculated using the following equation (equivalent to Eq. (1)):

$$\alpha_{rad} = \frac{\lambda_{POST} - \lambda_{PRE}}{\lambda_{PRE}(\bar{P}_{POST} - \bar{P}_{PRE})} \qquad (4)$$

where λ_{PRE} and λ_{POST} are the radial stretches obtained from the stress–stretch curve at baseline pressure ($\bar{P}_{PRE}$) and after embolization ($\bar{P}_{POST}$), respectively.

Statistical Analysis. For both angiographic techniques, one set of distensibility measurements was obtained from each animal. Statistical analysis was performed on these six datasets. All results are presented as mean $\pm$ standard error (SE). The relative difference between the two methods is calculated as the absolute value of the difference divided by the value obtained from CE-MRA. Changes in α along the six PA generations included in this study were analyzed using a linear mixed-effect model with repeated measures (generalized least squares). An autoregressive correlation structure was assumed between repeated measurements. Tukey's honestly significant differences were used as a posthoc test of significance. Comparison between data obtained from CT-DSA and CE-MRA was performed using a two-tailed paired Student's t-test. The same test was used to compare PA diameters from either angiographic technique with data from 2D PC MRI, and to compare distensibility data in vivo with data from ex vivo mechanical tests. A probability value $p < 0.05$ was considered evidence of statistical difference.

Results

PA Distensibility In Vivo. Measurements of PA diameter at baseline (PRE) and radial distensibility α_{rad} for each branch generation from both CT-DSA and CE-MRA are shown in Table 1. For the RPA, the average values of α_{rad} ranged between 1.47% and 2.63%/mmHg when calculated from CT-DSA data, and between 1.81% and 2.29%/mmHg when calculated from CE-MRA data. For the LPA, the average α_{rad} ranged between 1.49% and 2.17%/mmHg (CT-DSA) and between 1.99% and 3.33%/mmHg (CE-MRA). None of the branches from second to sixth generation had distensibility significantly different from the first branch generation (both RPA and LPA). We found no statistical differences between the results from the two angiographic techniques, with the only exception of the third branch generation of the LPA, where CE-MRA-based α_{rad} was significantly larger than CT-DSA.

Table 2 reports the values of PA branch length at baseline (PRE) and axial distensibility α_{ax} for all branch generations. Average α_{ax} for both LPA and RPA ranged between slightly negative values to positive values, consistently lower than α_{rad}. Axial distensibility was generally lower in generations 2–6 compared to the first generation, although the trend was significant only in the LPA (from CT-DSA data) and in few isolated cases. We found no significant difference between α_{ax} estimated from CT-DSA and CE-MRA.

Comparison With PC MRI. We compared the radial distensibility α_{rad} calculated from CT-DSA and CE-MRA with calculations from PC MRI data. Only first branch generation data (LPA and RPA) were available from PC MRI. Radial distensibility values from PC MRI tended to be smaller than those obtained from either angiographic technique, but we found no significant differences among imaging methods (Table 3).

Comparison With Ex Vivo Mechanical Tests. We also compared the radial distensibility α_{rad} calculated from ex vivo mechanical tests with those obtained from angiographic and PC MRI methods; again, only first branch generation data (LPA and RPA) were available from ex vivo tests. Ex vivo estimates of α_{rad} tended to be lower than in vivo angiographic measurements, and in one case (CT-DSA-based estimate of α_{rad} for the RPA) the difference was statistically significant (Table 3).

Resolution Limits. In order to be captured by the in vivo approach proposed here, changes in length or diameter of the PA branches should be larger than the spatial resolution limits of the

Table 1 PA branch average diameter at baseline (PRE) and radial distensibility for the six generations of RPA and LPA branches, estimated from CT-DSA and CE-MRA data. For each branch generation of RPA and LPA, the relative difference in α_{rad} between the two methods is included.

Branch generation		Radial distensibility					
		1	2	3	4	5	6
	RPA						
D_{PRE} (mm)	CT-DSA	8.71 ±0.42	7.52 ± 0.45†	6.95 ± 0.27†	5.35 ± 0.28†	4.02 ±0.31†	2.43 ±0.21†
	CE-MRA	7.81 ±0.29	6.99 ± 0.29†	6.57 ± 0.26†	5.40 ± 0.38†	4.41 ± 0.49†	3.29 ±0.55†
α_{rad}(%mmHg)	CT-DSA	2.42 ±0.42	2.63 ±0.56	1.56 ±0.30	1.47 ±0.31	1.76 ±0.39	2.10±0.48
	CE-MRA	2.29 ±0.40	2.23 ±0.41	1.81 ±0.35	1.84 ±0.44	2.10 ±0.54	2.11±0.62
	$\Delta\alpha_{rad}/\alpha_{rad,CE-MRA}$	0.53 ±0.20	0.66 ±0.53	0.30 ±0.08	0.56 ±022	0.35 ±0.08	0.64 ±0.11
	LPA						
D_{PRE} (mm)	CT-DSA	8.05 ±0.30	7.35 ± 0.35†	7.24 ± 0.54†	5.67 ± 0.29†	4.29 ± 0.32†	2.61 ± 0.37†
	CE-MRA	6.85 ± 0.28*	6.55 ± 0.20	5.92 ± 0.12†	5.28 ± 0.26†	3.76 ± 0.36†	2.66 ± 0.37†
α_{rad}(%mmHg)	CT-DSA	2.17 ±0.31	2.14±0.45	1.79 ±0.64	1.61 ±0.42	1.49 ±0.38	1.91 ±0.62
	CE-MRA	2.30 ±0.43	2.15 ±0.47	2.34 ± 0.59*	1.99 ±0.38	2.51 ±0.62	3.33 ±0.90
	$\Delta\alpha_{rad}/\alpha_{rad,CE-MRA}$	0.33 ±0.09	0.62 ±0.39	0.31 ±0.12	0.54 ±0.12	0.43 ±0.09	0.63 ±0.08

Values are expressed as mean ± SE.
*$p < 0.05$, compared to CT-DSA;
†$p < 0.05$, compared to the first branch generation.

Table 2 PA branch length at baseline (PRE) and axial distensibility for the six generations of RPA and LPA branches, estimated from CT-DSA and CE-MRA data. For each branch generation of RPA and LPA, the relative difference in α_{ax} between the two methods is included.

Branch generation		Axial distensibility					
		1	2	3	4	5	6
	RPA						
L_{PRE} (mm)	CT-DSA	14.33 ± 0.95	31.19 ± 1.07†	44.97 ± 2.04†	62.23 ± 3.02†	83.25 ± 3.80	112.68 ± 3.82†
	CE-MRA	9.75 ±1.56	25.35 ± 2.66†	38.61 ± 3.35†	50.85 ± 5.37†	67.18 ± 7.37†	104.95 ± 2.42†
α_{ax}(%/mmHg)	CT-DSA	1.11 ±0.58	−0.29 ± 0.29†	0.32 ±0.12	−0.06 ± 0.05	0.11 ±0.04	−0.07 ±0.12†
	CE-MRA	1.88 ±0.49	0.42 ±0.63	−0.13 ±0.17†	0.04 ±0.06	0.21 ±0.15	0.74 ±0.92
	$\Delta\alpha_{ax}/\alpha_{ax,CE-MRA}$	0.65 ±0.19	2.04 ±0.67	2.04 ±0.98	1.97 ±0.37	1.08 ±0.33	0.95 ±024
	LPA						
L_{PRE} (mm)	CT-DSA	6.22 ±0.60	15.55 ± 2.27†	22.32 ± 0.96†	35.86 ± 1.67†	53.94 ± 3.74†	82.83 ± 1.87†
	CE-MRA	5.26 ±1.47	14.42 ± 3.26†	20.13 ± 0.96†	33.88 ± 2.98†	48.08 ± 3.84†	81.08 ±4.71†
α_{ax} (%/mmHg)	CT-DSA	1.54 ±0.33	−0.01 ± 0.27†	0.33 ±0.30	−0.00 ± 0.13†	0.43 ±0.27†	−0.33 ±0.28†
	CE-MRA	0.57 ±0.56	1.30 ±0.27*	0.27 ±0.50	−0.35 ±0.19	−0.06 ±0.10	−0.28 ±0.32
	$\Delta\alpha_{ax}/\alpha_{ax,CE-MRA}$	1.38 ±0.64	0.95 ±0.23	1.67 ±0.99	1.61 ±038	2.53 ±0.64	0.85 ±037

Values are expressed as mean ± SE.
*$p < 0.05$, compared to CT-DSA;
†$p < 0.05$, compared to the first branch generation.

imaging technique. We compared the average dilatation (Fig. 2) and elongation (Fig. 3) of each branch of LPA and RPA with the resolution limit of CE-MRA, which is the technique with the poorer spatial resolution (1.5 mm). Figure 2 illustrates that the acute pressure increase resulted in values of PA branch dilatation above the resolution limit, with the exception of the sixth branch

Table 3 Radial distensibility for RPA and LPA (first branch generation), measured in vivo (CT-DSA, CE-MRA, PC MRI) and ex vivo (mechanical tests).

Branch	Radial distensibility, α_{rad} (%/mmHg)	
	RPA	LPA
CT-DSA	2.42 ± 0.42†	2.17 ± 0.31
CE-MRA	2.29 ± 0.40	2.30 ± 0.43
PC MRI	1.59 ± 0.50	1.89 ± 0.62
Mechanical tests	1.64 ± 0.22	1.74 ± 0.29

Values are expressed as mean ± SE.
*$p < 0.05$, compared to PC MRI;
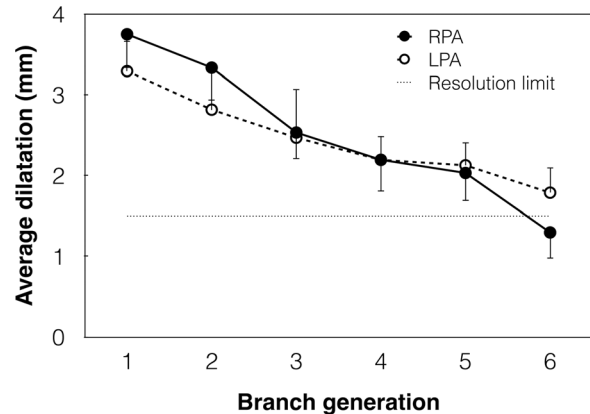†$p < 0.05$, compared to mechanical tests.

Fig. 2 Change in average diameter of the six branch generations of RPA (*solid line*) and LPA (*dashed line*) from PRE to POST. Error bars show the SE. The straight dotted line represents the spatial resolution limit of CE-MRA (1.5 mm).
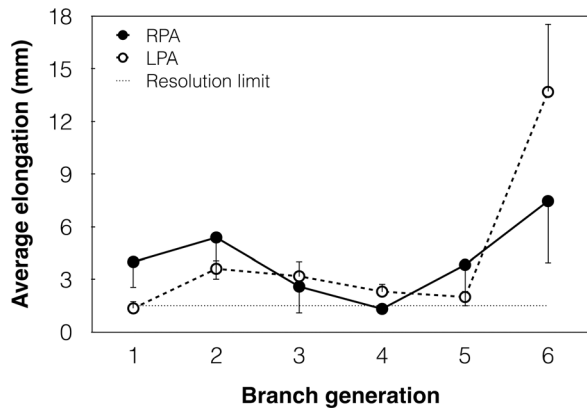
Fig. 3 Change in length of the six branch generations of RPA (*solid line*) and LPA (*dashed line*) from PRE to POST. Error bars show the SE. The straight dotted line represents the spatial resolution limit of CE-MRA (1.5 mm).

generation, whose dilatation is of the same order of the resolution limit. Branch elongation data are also generally above the resolution limit, with the exception of the first generation of LPA and fourth generation of RPA (Fig. 3).

Discussion

In this study we present a novel in vivo approach to estimate distensibility of individual branches of the PA network. To the best of our knowledge, this is the first method that allows for in vivo assessment of compliance properties of arterial branches distal to the first generation (LPA and RPA). Additionally, our method can be used to assess both radial and axial distensibility.

Combining invasive PA pressure measurements with angiographic imaging of the pulmonary vasculature has potential clinical application. CT-DSA can be performed during RHC [25], so that hemodynamic and structural data can be obtained simultaneously. In contrast, methods based on simultaneous MRI and RHC have only been used in pilot studies and are not yet established clinical research tools [26–29].

To assess PA distensibility from the slope of the diameter–pressure relationship, our approach requires that data be obtained at two different PA stretch levels. In our preclinical study, we used acute embolization to alter the mean pressure in the PAs. In future clinical applications of our method, an acute increase in PA pressure can be obtained via physical exercise, taking advantage of the positive relationship between cardiac output and PA pressure [30]. Alternatively, PA pressure can be temporarily increased via dobutamine infusion, which is often done clinically for stress testing [31,32].

Previous studies, based on the distensibility model proposed by Linehan [12], determined that the radial distensibility of the PA network measured globally, and assumed constant throughout, is approximately ∼2%/mmHg [16,17]. Unlike Linehan's method, our approach measures the distensibility of individual branches of the PA network. According to our results, each PA branches down to the sixth generation has radial distensibility close to ∼2%/mmHg, thus supporting the Linehan model. However, whether the decrease in PA network distensibility observed in patients with PAH [13] is consistent in all the PAs down to 1–2 mm diameter (the spatial resolution limit of our angiographic methods) remains unknown. Future clinical application of our method will address this knowledge gap. In addition, our approach can be used to investigate the contribution of individual arterial branches to sex-related difference in PA distensibility observed in healthy subjects [33].

This study was the first to assess axial distensibility in the pulmonary vasculature. Axial distensibility was markedly lower than radial distensibility, with the significant exception of the first branch generation (LPA and RPA), which distended comparably in both radial and axial directions. We speculate that PA branches distal to the first generation had limited ability to distend axially due to the effects of tethering forces, spatial constraints in the chest cavity and external pressure from inflated alveoli.

Both CT-DSA and CE-MRA can be used clinically to obtain a spatially resolved time-averaged representation of the pulmonary vasculature. Our results indicate that the two imaging methods provide comparable radial and axial distensibilities. In addition, the two methods similarly tended to overestimate radial distensibility in the first branch generation (LPA and RPA), where a comparison was possible with PC MRI and with ex vivo mechanical tests. Therefore, accuracy should not be a deciding factor when selecting the angiographic method to assess PA distensibility. The main advantage of CE-MRA is the absence of ionizing radiation, whereas CT-DSA can be performed simultaneously with RHC.

Several limitations in this study must be acknowledged. The spatial resolution of both angiographic methods used here was approximately 1 mm, which limited the scope of our analysis to the first six branch generations. For these branch generations, in our experimental model the pressure increase induced changes in arterial diameter and length above the spatial resolution limit of the imaging techniques. This is not a limitation intrinsic to our method and future extension of distensibility measurements to smaller arteries (via improved imaging resolution) may have important clinical implications because of the significant contribution of smaller PAs to the total arterial distensibility [11]. We used the same value of pressure, measured invasively in the main PA only (zeroth generation), for all the branches included in our analysis, therefore neglecting possible spatial variations in pressure. Also, to calculate distensibility, we assumed a linear relationship between PA diameter (normalized to baseline) and pressure. Since the relationship is slightly curvilinear [30], future clinical applications of our method should include measurements at more than two pressure levels, either via incremental exercise or via progressive increase in dobutamine dosage. Finally, our uniaxial mechanical tests are an approximation of the actual biaxial loading experienced by the PAs in vivo. Inflation–extension tests are a more realistic representation of the physiological loading [34] and would provide a better validation of our in vivo measurements.

Conclusions

We presented an in vivo method to assess both axial and radial distensibility in the large and intermediate PAs. For the first time, this method allows for measuring mechanical properties of individual branches distal to the first generation. Our results indicate that large and intermediate PA branches have comparable radial distensibility, close to the 2%/mmHg value previously estimated for the entire PA network. Computed tomography angiography and magnetic resonance angiography provide comparable results. Established in vivo and ex vivo methods, which can only be used in the first branch generation, provided a preliminary validation of our novel approach.

Acknowledgment

References

[1] Hunter, K. S., Lee, P.-F., Lanning, C. J., Ivy, D. D., Kirby, K. S., Claussen, L. R., Chan, K. C., and Shandas, R., 2008, "Pulmonary Vascular Input Impedance is a Combined Measure of Pulmonary Vascular Resistance and Stiffness and Predicts Clinical Outcomes Better Than Pulmonary Vascular Resistance Alone in Pediatric Patients With Pulmonary Hypertension," Am. Heart J., **155**(1), pp. 166–174.

[2] Mahapatra, S., Nishimura, R. A., Sorajja, P., Cha, S., and McGoon, M. D., 2006, "Relationship of Pulmonary Arterial Capacitance and Mortality in Idiopathic Pulmonary Arterial Hypertension," J. Am. Coll. Cardiol., **47**(4), pp. 799–803.

[3] Ooi, C. Y., Wang, Z., Tabima, D. M., Eickhoff, J. C., and Chesler, N. C., 2010, "The Role of Collagen in Extralobar Pulmonary Artery Stiffening in Response to Hypoxia-Induced Pulmonary Hypertension," Am. J. Physiol. Heart Circ. Physiol., **299**(6), pp. H1823–H1831.

[4] Gan, C. T.-J., Lankhaar, J.-W., Westerhof, N., Marcus, J. T., Becker, A., Twisk, J. W. R., Boonstra, A., Postmus, P. E., and Vonk-Noordegraaf, A., 2007, "Noninvasively Assessed Pulmonary Artery Stiffness Predicts Mortality in Pulmonary Arterial Hypertension," Chest, **132**(6), pp. 1906–1912.

[5] Sanz, J., Kariisa, M., Dellegrottaglie, S., Prat-González, S., Garcia, M. J., Fuster, V., and Rajagopalan, S., 2009, "Evaluation of Pulmonary Artery Stiffness in Pulmonary Hypertension With Cardiac Magnetic Resonance," JACC Cardiovasc. Imaging, **2**(3), pp. 286–295.

[6] D'Alonzo, G. E., Barst, R. J., Ayres, S. M., Bergofsky, E. H., Brundage, B. H., Detre, K. M., Fishman, A. P., Goldring, R. M., Groves, B. M., and Kernis, J. T., 1991, "Survival in Patients With Primary Pulmonary Hypertension. Results From a National Prospective Registry," Ann. Intern. Med., **115**(5), pp. 343–349.

[7] Dodson, R. B., Morgan, M., Galambos, C., Hunter, K. S., and Abman, S. H., 2014, "Chronic Intrauterine Pulmonary Hypertension Increases Main Pulmonary Artery Stiffness and Adventitial Remodeling in Fetal Sheep," Am. J. Physiol. Lung Cell. Mol. Physiol., **307**(11), pp. L822–L828.

[8] Swift, A. J., Rajaram, S., Condliffe, R., Capener, D., Hurdman, J., Elliot, C., Kiely, D. G., and Wild, J. M., 2012, "Pulmonary Artery Relative Area Change Detects Mild Elevations in Pulmonary Vascular Resistance and Predicts Adverse Outcome in Pulmonary Hypertension," Invest. Radiol., **47**(10), pp. 571–577.

[9] Su, Z., Tan, W., Shandas, R., and Hunter, K. S., 2013, "Influence of Distal Resistance and Proximal Stiffness on Hemodynamics and RV Afterload in Progression and Treatments of Pulmonary Hypertension: A Computational Study With Validation Using Animal Models," Comput. Math. Methods Med., **2013**, p. 618326.

[10] Su, Z., Hunter, K. S., and Shandas, R., 2012, "Impact of Pulmonary Vascular Stiffness and Vasodilator Treatment in Pediatric Pulmonary Hypertension: 21 Patient-Specific Fluid–Structure Interaction Studies," Comput. Methods Programs Biomed., **108**(2), pp. 617–628.

[11] Saouti, N., Westerhof, N., Helderman, F., Marcus, J. T., Stergiopulos, N., Westerhof, B. E., Boonstra, A., Postmus, P. E., and Vonk-Noordegraaf, A., 2009, "RC Time Constant of Single Lung Equals That of Both Lungs Together: A Study in Chronic Thromboembolic Pulmonary Hypertension," Am. J. Physiol. Heart Circ. Physiol., **297**(6), pp. H2154–H2160.

[12] Linehan, J. H., Haworth, S. T., Nelin, L. D., Krenz, G. S., and Dawson, C. A., 1992, "A Simple Distensible Vessel Model for Interpreting Pulmonary Vascular Pressure-Flow Curves," J. Appl. Physiol., **73**(3), pp. 987–994.

[13] Blyth, K. G., Syyed, R., Chalmers, J., Foster, J. E., Saba, T., Naeije, R., Melot, C., and Peacock, A. J., 2007, "Pulmonary Arterial Pulse Pressure and Mortality in Pulmonary Arterial Hypertension," Respir. Med., **101**(12), pp. 2495–2501.

[14] Argiento, P., Chesler, N., Mulè, M., D'Alto, M., Bossone, E., Unger, P., and Naeije, R., 2010, "Exercise Stress Echocardiography for the Study of the Pulmonary Circulation," Eur. Respir. J., **35**(6), pp. 1273–1278.

[15] Vanderpool, R. R., Kim, A. R., Molthen, R., and Chesler, N. C., 2011, "Effects of Acute Rho Kinase Inhibition on Chronic Hypoxia-Induced Changes in Proximal and Distal Pulmonary Arterial Structure and Function," J. Appl. Physiol., **110**(1), pp. 188–198.

[16] Reeves, J. T., Linehan, J. H., and Stenmark, K. R., 2005, "Distensibility of the Normal Human Lung Circulation During Exercise," Am. J. Physiol. Lung Cell. Mol. Physiol., **288**(3), pp. L419–L425.

[17] Krenz, G. S., and Dawson, C. A., 2003, "Flow and Pressure Distributions in Vascular Networks Consisting of Distensible Vessels," Am. J. Physiol. Heart Circ. Physiol., **284**(6), pp. H2192–H2203.

[18] Scott-Drechsel, D., Su, Z., Hunter, K., Li, M., Shandas, R., and Tan, W., 2012, "A New Flow Co-Culture System for Studying Mechanobiology Effects of Pulse Flow Waves," Cytotechnology, **64**(6), pp. 649–666.

[19] Morrell, N. W., 2006, "Pulmonary Hypertension Due to BMPR2 Mutation: A New Paradigm for Tissue Remodeling?," Proc. Am. Thorac. Soc., **3**(8), pp. 680–686.

[20] Pavelescu, A., Vanderpool, R., Vachiéry, J.-L., Grunig, E., and Naeije, R., 2012, "Echocardiography of Pulmonary Vascular Function in Asymptomatic Carriers of BMPR2 Mutations," Eur. Respir. J., **40**(5), pp. 1287–1289.

[21] Naeije, R., 2013, "Physiology of the Pulmonary Circulation and the Right Heart," Curr. Hypertens. Rep., **15**(6), pp. 623–631.

[22] Bellofiore, A., Roldán-Alzate, A., Besse, M., Kellihan, H. B., Consigny, D. W., Francois, C. J., and Chesler, N. C., 2013, "Impact of Acute Pulmonary Embolization on Arterial Stiffening and Right Ventricular Function in Dogs," Ann. Biomed. Eng., **41**(1), pp. 195–204.

[23] Kalender, W. A., and Kyriakou, Y., 2007, "Flat-Detector Computed Tomography (FD-CT)," Eur. Radiol., **17**(11), pp. 2767–2779.

[24] Kamran, M., Nagaraja, S., and Byrne, J. V., 2010, "C-Arm Flat Detector Computed Tomography: The Technique and Its Applications in Interventional Neuro-Radiology," Neuroradiology, **52**(4), pp. 319–327.

[25] Raman, S. V., Tran, T., Simonetti, O. P., and Sun, B., 2009, "Dynamic Computed Tomography to Determine Cardiac Output in Patients With Left Ventricular Assist Devices," J. Thorac. Cardiovasc. Surg., **137**(5), pp. 1213–1217.

[26] Rogers, T., Ratnayaka, K., and Lederman, R. J., 2014, "MRI Catheterization in Cardiopulmonary Disease," Chest, **145**(1), pp. 30–36.

[27] Ratnayaka, K., Faranesh, A. Z., Hansen, M. S., Stine, A. M., Halabi, M., Barbash, I. M., Schenke, W. H., Wright, V. J., Grant, L. P., Kellman, P., Kocaturk, O., and Lederman, R. J., 2013, "Real-Time MRI-Guided Right Heart Catheterization in Adults Using Passive Catheters," Eur. Heart J., **34**(5), pp. 380–389.

[28] Muthurangu, V., Atkinson, D., Sermesant, M., Miquel, M. E., Hegde, S., Johnson, R., Andriantsimiavona, R., Taylor, A. M., Baker, E., Tulloh, R., Hill, D., and Razavi, R. S., 2005, "Measurement of Total Pulmonary Arterial Compliance Using Invasive Pressure Monitoring and MR Flow Quantification During MR-Guided Cardiac Catheterization," Am. J. Physiol. Heart Circ. Physiol., **289**(3), pp. H1301–H1306.

[29] Kuehne, T., Yilmaz, S., Steendijk, P., Moore, P., Groenink, M., Saaed, M., Weber, O., Higgins, C. B., Ewert, P., Fleck, E., Nagel, E., Schulze-Neick, I., and Lange, P., 2004, "Magnetic Resonance Imaging Analysis of Right Ventricular Pressure–Volume Loops," Circulation, **110**(14), pp. 2010–2016.

[30] Naeije, R., and Chesler, N., 2012, "Pulmonary Circulation at Exercise," Compr. Physiol., **2**(1), pp. 711–741.

[31] Graham, R., Skoog, C., Macedo, W., Carter, J., Oppenheimer, L., Rabson, J., and Goldberg, H. S., 1983, "Dopamine, Dobutamine, and Phentolamine Effects on Pulmonary Vascular Mechanics," J. Appl. Physiol., **54**(5), pp. 1277–1283.

[32] Borlaug, B. A., Melenovsky, V., Marhin, T., Fitzgerald, P., and Kass, D. A., 2005, "Sildenafil Inhibits Beta-Adrenergic-Stimulated Cardiac Contractility in Humans," Circulation, **112**(17), pp. 2642–2649.

[33] Argiento, P., Vanderpool, R. R., Mule, M., Russo, M. G., D'Alto, M., Bossone, E., Chesler, N. C., and Naeije, R., 2012, "Exercise Stress Echocardiography of the Pulmonary Circulation: Limits of Normal and Gender Differences," Chest, **142**(5), pp. 1158–1165.

[34] Tian, L., and Chesler, N. C., 2012, "In Vivo and In Vitro Measurements of Pulmonary Arterial Stiffness: A Brief Review," Pulm. Circ., **2**(4), pp. 505–517.